Shape resonances and multielectron effects in the core-level photoionization of CO_2

M. Schmidbauer,* A. L. D. Kilcoyne, H.-M. Köppe, J. Feldhaus,† and A. M. Bradshaw
Fritz-Haber-Institut der Max-Planck-Gesellschaft, Faradayweg 4-6, 14195 Berlin, Germany
(Received 6 February 1995)

The partial photoionization cross sections and angular distributions of the C $1s^{-1}$ and O $1s^{-1}$ single-hole states of CO_2 have been measured with high precision near threshold. The $4\sigma_u^*$ shape resonance is well reproduced in the $1s$ single-hole cross sections, but strong site-specific effects are observed with respect to both its energy and intensity. A striking feature of the present data is the presence of fine structure in the $1s$ single-hole cross sections σ_{SH} due to multielectron excitations: virtually all spectral details in the total $1s$ cross sections σ_{1s} are also present in σ_{SH} implying that multielectron excitations couple strongly to the underlying $1s$ continuum. The decay dynamics of the double-excitation feature at 303.5 eV in the C $1s$ cross section of CO_2 have been characterized by Auger spectroscopy. Partial cross sections and angular distributions have also been measured for the first group of strong shake-up satellites in the C $1s$ photoelectron spectrum. Similar to the C $1s$ ionization of CO, a strong enhancement of intensity near threshold is observed for some satellite channels as well as the occurrence of features that are not present in the sudden limit. The latter are attributed to conjugate shake-up.

PACS number(s): 33.80.Eh, 33.60.Fy

I. INTRODUCTION

A considerable body of experimental and theoretical work on photoabsorption and photoionization cross sections has shown that resonances and multielectron effects are commonly encountered in core-level excitation of small molecules. In some studies these features have been carefully characterized and provide models for the interpretation of similar effects in larger molecules [1,2]. The current upsurge of interest in such K-shell properties is due to recently improved instrumentation, in particular high-resolution monochromators in combination with undulator sources, for absorption and photoelectron spectroscopy experiments, e.g., [3–6]. These allow detailed examination of the energetics and dynamics of core-level photoionization.

The excitation of a core electron into an unoccupied bound molecular orbital or the continuum is generally accomplished by a strong relaxation of the remaining system of charges. Provided that sufficient energy is available from the absorbed photon, there is a relatively high probability that a valence electron and vibrations are excited simultaneously with the core electron, giving rise to shake-up satellites in the photoelectron spectra [7–10] and to vibrational structure in both photoabsorption [3–5] and photoemission spectra [6,11]. Transitions to unoccupied states accompanied by shake-up often produce characteristic features in the continuum just below the onset of the shake-up satellites seen in the photoelectron spectra and have been referred to as double excitations. In the same energy region, i.e., within the first tens of eV above the core ionization threshold, a broad resonance is characteristically found in the photoabsorption spectra of small molecules, commonly referred to as a shape resonance [1]. In contrast to the shake-up process, it is inherently a one-electron phenomenon and is due to the temporary trapping of the outgoing photoelectron by a centrifugal potential barrier or, in an alternative description, due to a transition into an antibonding molecular orbital in the continuum [12]. Although the basic phenomenon is quite well understood, there have been only a few detailed experimental studies on core-level shape resonances. Generally speaking, only qualitative agreement is found between theory and experiment; even for simple diatomics there are large discrepancies with regard to the energetic position, the strength, and the detailed shape of the resonance.

In polyatomic molecules, the effects caused by the different dynamic relaxation of the valence electrons upon ionization of the different core levels and the selective probing of the continuum wave function by the localized core holes are particularly interesting. The shape resonance profile can be different, depending on which atomic core level is ionized. Moreover, more than one resonance is generally present (e.g., in valence ionization), so that not only the spatial localization but also the symmetry properties of the shape resonances become important [13–16]. A prominent example of the occurrence of such effects is provided by N_2O [13]. Core-level photoionization in CO_2 (O—C—O) is expected to have many of the features of that in N_2O (N—N—O), despite the different point-group symmetry: both molecules are linear, isoelectronic, and, in particular, their valence orbitals are strongly delocalized. Two shape resonances have been predicted by theory for the core levels of CO_2 [17,18], corresponding to transitions into the virtual antibonding $5\sigma_g^*$ and $4\sigma_u^*$ molecular orbitals. However, dipole selection rules allow only the $4\sigma_u^*$ resonance for C $1s$ ($2\sigma_g$ orbital) photoionization, whereas both resonances

*Present address: Max-Planck-Arbeitsgruppe "Röntgenbeugung," Hausvogteiplatz 5-7, 10117 Berlin, Germany.
†Present address: Hamburger Synchrotronstrahlungslabor at DESY, Notkestraße 85, 22603 Hamburg, Germany.

can occur for O 1s ($1\sigma_g, 1\sigma_u$) photoionization.

The identification of the characteristic features due to double and multielectron excitations requires a detailed examination of photoabsorption spectra at high resolution [3,4,19] and/or of the corresponding data from electron-energy-loss spectroscopy (EELS) [20,21]. In the total photoabsorption (photoionization) cross section of CO_2 above the C 1s threshold, there is additional fine structure due to multielectron excitations superimposed on the broad $4\sigma_u^*$ shape resonance. Particularly noticeable are two narrow features at 303.5 and 553 eV photon energy (i.e., just above the C 1s and O 1s thresholds, respectively). Similar features have been observed in the total cross sections (EELS) of other small low-Z molecules such as CO [21], N_2 [21], N_2O [20], C_2H_2 [22], C_2H_4 [22], and C_6H_6 [22]. However, many of these studies were performed with only moderate-energy resolution and so far high-resolution photoabsorption spectra of this region have only been measured for CO and N_2 [3–5,19]. For C 1s in CO it was shown that a feature in the absorption cross section at about 301 eV consists of states of the type $1s^{-1}v_1^{-1}v_2^1R^1$, where v denotes a valence state and R a Rydberg state, which are part of one or more Rydberg series of doubly excited states converging on satellite onsets [19,23]. In a recent study of C 1s photoionization of CO and CO_2 [24], we demonstrated that these doubly excited states strongly couple to the C $1s^{-1}$ continuum and thus influence the C $1s^{-1}$ single-hole cross sections and the corresponding asymmetry parameters. This coupling opens an alternative decay channel for these doubly excited states, in addition to the direct ("resonant") Auger process where only the fast resonant Auger electron is emitted. They first autoionize into the 1s continuum and then decay via a "normal" Auger process, thus emitting two electrons—a slow photoelectron and a normal Auger electron.

Previous work on the simple diatomic molecules CO and N_2 have also shown very interesting energy-dependent behavior of the satellites, as well as the occurrence of new satellites at energies close to threshold that cannot be predicted within the simple adiabatic picture [9,25–27]. The latter are not due to direct shake-up processes, but rather to a conjugate shake-up mechanism whereby a discrete dipole excitation of the core electron is accompanied by a "shake-off" of a valence electron. In contrast, in the normal shake-up process, dipole ionization of the core electron is accompanied by a monopole excitation of a valence electron. Theory [10,28] has shown that for very high photoelectron kinetic energies conjugate processes can be neglected and that only the direct part of the transition amplitude contributes to the satellite intensity, the latter accounting for typically 30–40 % of the partial 1s cross section in the "sudden limit." At low photoelectron kinetic energies, conjugate shake-up may become potentially as important as direct shake-up and can make a non-negligible contribution to the total shake-up intensity. This can result in an increasing rather than a decreasing satellite intensity as threshold is approached [29], in contrast to the simple adiabatic picture. Moreover, additional, so-called *pure conjugate* satellites may arise due to the different selection rules governing these processes near threshold, so that excited states of the ion with different symmetry become accessible [23,28].

In the C 1s photoionization of CO, the different behavior of the singlet and triplet coupled π-π^* $^2\Sigma^+$ satellites as a function of photon energy, for example, is interpreted as being due to an interference effect between the direct and the conjugate parts of the transition amplitude. In addition, it has also been established that several pure conjugate satellites are present in the C 1s photoelectron spectrum [23,30–32]. One complication of this picture, however, is that shape resonances can also be present in satellite continuum channels, as has been suggested for the C 1s satellites of C_2H_4 [14], H_2CO [14], and CO [23,26,27,30], so that shape resonant enhancement and conjugate processes cannot necessarily be distinguished in a photon energy-dependent experiment. This problem led to contradictory interpretations of the near-threshold energy-dependent behavior of the C 1s satellites of CO, where both models were cited in order to explain the different behavior of the singlet and triplet coupled π-π^* $^2\Sigma^+$ satellites [26,27]. In contrast, studies on noble gases have clearly shown the importance of conjugate processes [33,34]. The core-level satellites of CO_2 have been previously observed using Mg $K\alpha$ ($h\nu$=1254 eV) [7] and Al $K\alpha$ ($h\nu$=1486.6 eV) [35] radiation. These spectra may be compared with calculations using a fourth-order algebraic diagrammatic construction [ADC(4)] scheme by Angonoa and Schirmer [36], who assign the most prominent satellites and give their relative intensity. So far, no photon energy dependence has been measured.

This discussion shows that the measurement of the partial cross sections and angular distributions for the main lines as well as the satellites is important for a deeper understanding of shape resonance behavior and of the contribution of double- and multiple-electron excitations. Here we complement our previous investigations on other small molecules [13,14,24] by studying photoionization from both the C and O 1s core levels of CO_2 and comparing, where appropriate, with the studies on N_2O and CO. In Sec. II we briefly describe the experimental setup and our data analysis procedure. In Sec. III we consider the single-hole cross sections and angular distributions and compare the curves with the available theory. A preliminary account of this work has appeared in Ref. [24]. The question of double- and multiple-electron excitations is then considered in detail in Sec. IV. An analysis of the C 1s satellite structure follows in Sec. V. Section VI describes a resonant Auger spectra study of multiexcited states for C 1s, which extends the information obtained from the main and satellite lines. Finally, the results are summarized in Sec. VII.

II. EXPERIMENT

The photoelectron spectrometer used in this study consisted of a stationary angle-resolving magic-angle cylindrical mirror analyzer (CMA) with its axis collinear with the incoming synchrotron radiation beam. The analyzer includes a preacceleration lens that defines, together with a conical gas inlet configuration, the acceptance angle of

the electrons. In this geometry, the total intensity is independent of the angular distribution of the photoelectrons and the degree of light polarization and can therefore be used to determine the partial photoionization cross sections σ. The angular distribution of the photoelectrons and the degree of light polarization can, however, be simultaneously determined by utilizing the cylindrical symmetry in combination with a specially designed eightfold segmented detector and the known angular distributions from a rare gas. A complete description of the spectrometer has been published previously [37].

Photoelectron and Auger spectra were measured for CO_2 during three separate beam times and at two different facilities. The vacuum ultraviolet radiation was provided by the high-energy (HE) toroidal grating monochromator (TGM) [38] of the Fritz-Haber-Institut at the Berlin electron storage ring BESSY and the spherical grating monochromator on the X1B beam line [5] at the National Synchrotron Light Source (NSLS). The former monochromator is characterized by a spectral resolution that is better than 1 eV at the carbon K edge and about 2.5 eV at the oxygen K edge and a photon flux at the target gas of the order of 10^{10}–10^{11} photons per second. For the latter monochromator, the best energy resolution at the nitrogen K edge at $\sim$400 eV lies well below 70 meV and at the oxygen K edge it is $\sim$100 meV. This resolution, however, can only be achieved with small entrance and exit slits, resulting in a photon flux that is insufficient for photoelectron spectroscopy. Using larger slits the flux can be increased to more than 10^{11} photons per second, with a moderate decrease in energy resolution to $\sim$200 meV at the carbon K edge and $\sim$500 meV at the oxygen K edge.

All photoelectron spectra were recorded at a constant CMA pass energy of 80 eV, which is equivalent to a CMA bandwidth of $\sim$0.7 eV. Auger electrons were collected by tuning the pass energy. Typical count rates, with a target pressure in the interaction region of $\sim 10^{-2}$–10^{-3} mbar and 10^{-6} mbar at the detector, are of some thousand counts per second in the 1s main lines. Test spectra were taken to ensure that there was no observable pressure dependence of the peaks. The relative intensity of the monochromatic light as well as its degree of polarization were determined by recording 2s and 2p photoelectron spectra of Ne alternately with the CO_2 spectra. Using known Ne 2s and 2p cross sections and β parameters [37,39], the integrated intensities could be normalized to the photon flux and the angular distributions for the sample gas corrected. In addition, the transmission function of the CMA and lens configuration during each measuring period was determined by using the known photoionization cross sections for Ar [40] and Ne. Both Auger and photoelectron spectra were measured consecutively and normalized as indicated in Sec. III. The single-hole and satellite photoionization cross sections and the partial photoionization cross sections in the figures below are thus absolute and given in Mb.

The statistical error of the data is negligible (for the main lines) and within the size of the symbols used in the figures. At very low photoelectron kinetic energies the accuracy is limited by uncertainties in the CMA-lens transmission and by the background subtraction procedure [13]. The data recorded from the two different monochromators showed a high level of agreement between the different sets of cross sections and asymmetry parameters. Some indication of the error in the determination of partial cross sections can be obtained from Figs. 2(a) and 3(a), which show the scatter of the data points from different measurement series; the error in the asymmetry parameter is of the order of $\pm 0.1\ \beta$ units. At low kinetic energies the data from the X1B monochromator are more reliable because the better energy resolution, together with a highly collimated photon beam gave a reduced secondary-electron background and hence facilitated the background subtraction procedure used.

III. SINGLE-HOLE PHOTOIONIZATION CROSS SECTIONS AND ASYMMETRY PARAMETERS

Typical C 1s and O 1s photoelectron spectra for CO_2, measured at 330.7 and 574.1 eV photon energy, respectively, are shown in Figs. 1(a) and 1(b). They are dominated by the C 1s and O 1s main lines with binding energies of 297.5 and 540.8 eV, corresponding to the C $1s^{-1}$ and O $1s^{-1}$ single-hole states, respectively, and at lower kinetic energies by strong shake-up satellites due to

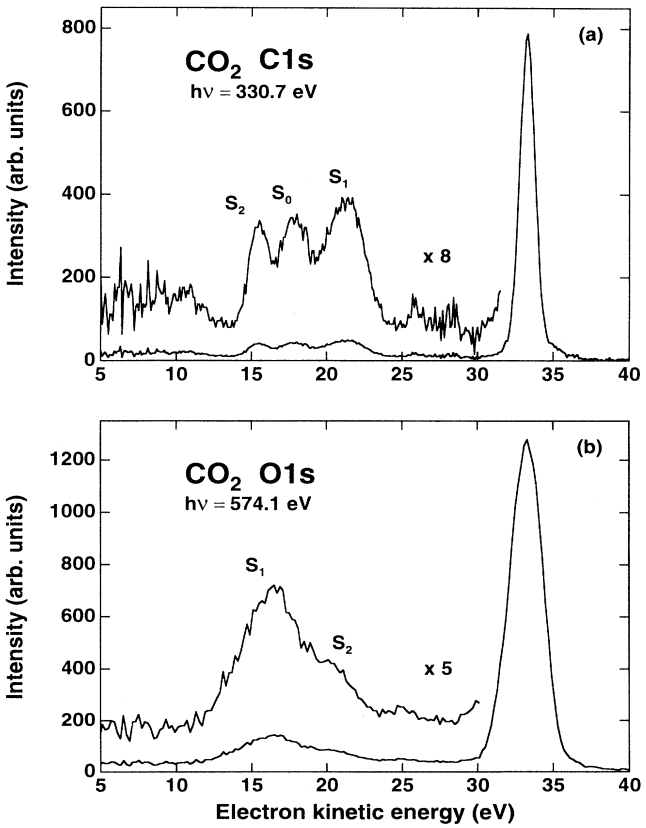

FIG. 1. Experimental CO_2 core-level photoelectron spectra. (a) C 1s main line and satellite lines recorded at $h\nu$=330.7 eV. (b) O 1s main line and satellite lines recorded at $h\nu$=574.1 eV. A smooth secondary electron background has been subtracted.

simultaneous excitation of valence electrons. At these photon energies, approximately 30 eV above the respective core ionization thresholds, three well-resolved satellites are dominant in the C 1*s* spectrum, whereas two broad overlapping satellites are indicated in the case of O 1*s*. Note that the data shown are from the HE TGM at BESSY. Both spectra are in agreement with results obtained previously at 1486.6 eV photon energy using monochromatized Al $K\alpha$ radiation with a linewidth of ~ 0.3 eV [35]. The satellites for the O 1*s* core level are, however, not clearly resolved; higher-resolution spectra taken on the X1B monochromator at this photon energy show somewhat more details, but the satellites are still broad [41].

The results for the C $1s^{-1}$ single-hole photoionization cross sections σ_{SH}(C) and the total Auger intensity, along with frozen core Hartree-Fock (FCHF) [42] and relaxed core Hartree-Fock (RCHF) [43] calculations, are shown in Fig. 2(a). Since the experimentally derived Auger intensity is proportional to the partial C 1*s* cross section σ_{1s}(C), it has been scaled to match the atomic carbon cross section [44] (equivalent to the values derived in EELS measurements [45,46]) at high photon energies. σ_{SH}(C) is then further adjusted relative to this curve, such that the difference properly accounts for the total shake-up and shake-off contribution. The latter is estimated to be 37% of the C 1*s* main line intensity σ_{SH}(C) at $h\nu = 320$ eV [47]. The data are in agreement with a previous measurement [48], but due to the lower scatter in our data, additional fine structure in the cross sections (and β parameters) are clearly visible. In particular, the double excitations at ~ 303.5 eV photon energy are well reproduced in the C 1*s* single-hole cross section σ_{SH}(C) in both sets of data (which were taken with the HE TGM at BESSY). At higher energies (~ 311 eV) both the C $1s^{-1}$ single-hole cross section σ_{SH}(C) and the total Auger intensity σ_{1s}(C) are dominated by a strong, broad enhancement due to the $4\sigma_u^*$ shape resonance. Superimposed on the shape resonance are additional features in both σ_{SH}(C) and σ_{1s}(C); these will be discussed below.

The corresponding data for the O 1*s* core level [σ_{SH}(O) and σ_{1s}(O)] together with the FCHF [42] and RCHF [43] calculations are shown in Fig. 3(a). In a way analogous to the C 1*s* data, the partial cross section was obtained by scaling to twice the atomic oxygen cross section [44] at high energy. For σ_{SH}(O), the curve was adjusted by estimating that 32% of the O 1*s* main line intensity at $h\nu = 570$ eV contributes to the satellite cross sections. It is immediately apparent that the O $1s^{-1}$ single-hole cross section σ_{SH}(O) has a significantly different profile compared to the EELS [22,45,46] and the total Auger intensity data σ_{1s}(O). In particular, the $4\sigma_u^*$ shape resonance is centered at ~ 561 eV in the single-hole cross section rather than at ~ 559 eV as in the partial cross section. The additional measurements for σ_{SH}(O) and σ_{1s}(O) on the X1B monochromator [with a finer energy mesh and higher resolution $\Delta E \sim 0.5$ eV, depicted in Fig. 3(a)] confirm the observation of different positions for the "resonance." Moreover, in all the experiments the single-hole and Auger spectra are acquired consecutively, without changing the energy position of the monochromator, so that the relative positions of the maxima appearing in the single-hole and total cross sections can be determined accurately. Note that the double-excitation feature at ~ 12 eV photoelectron energy is also confirmed by the measurements on X1B. The σ_{SH}(C) cross-section data at the lowest photon energies have a relatively large systematic error, making it difficult to verify the existence of the $5\sigma_g^*$ shape resonance indicated in the theoretical curves.

The asymmetry parameters β for C $1s^{-1}$ and O $1s^{-1}$ photoionization are shown in Figs. 2(b) and 3(b), respectively, and compared with FCHF [42] and RCHF [43] calculations. In the experimentally determined C 1*s* β values there is a broad oscillation with a maximum at 310 eV and a minimum at ~ 318 eV photon energy. In contrast, ionization from the O 1*s* level shows only a weak

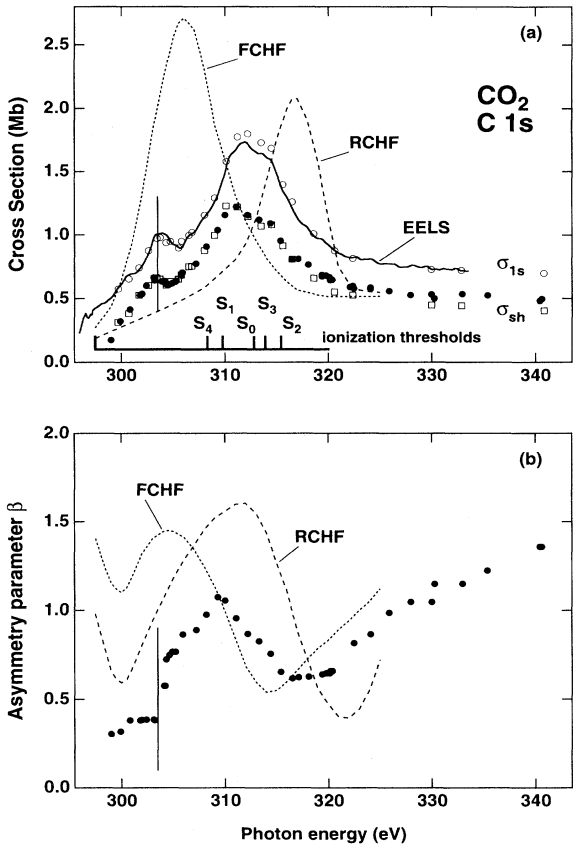

FIG. 2. (a) C 1*s* single-hole σ_{SH}(C) and partial σ_{1s}(C) photoionization cross section for CO_2. Two sets of measured data (● and □) are shown for the single-hole cross section, taken during two different measuring periods on the HE TGM monochromator. The total C 1*s* Auger intensity (○), which is proportional to the total C 1*s* cross section σ_{1s}(C), is compared to absolute EELS measurements (full line) [46]. The C 1*s* ionization threshold and the experimental thresholds of the lowest-shake-up satellites are indicated by bars below the curves. Also shown are calculations from McKoy and co-workers at the FCHF [42] and RCHF [43] levels. (b) Experimental C 1*s* asymmetry parameter β in comparison with FCHF [42] and RCHF [43] calculations.

oscillation that, in addition, is confined to a much narrower energy range. These differences demonstrate the site-specific probing of the resonant continuum wave function by the strongly localized core levels and in addition there might be some influence from the $5\sigma_g^*$ shape resonance at very low kinetic energies in O 1s ionization. The same qualitative behavior has been reported in N_2O [13], suggesting that the β-parameter curves of the central and terminal atoms are typical of photoionization of triatomic linear molecules in the vicinity of a delocalized continuum resonance. The oscillatory behavior is also evident in the HF calculations for both core levels, but there are clearly discrepancies between theory and experiment.

The shape resonance leads to a very strong maximum in the C 1s single-hole cross section, whereas in the case of O 1s only a weak enhancement is observed. This

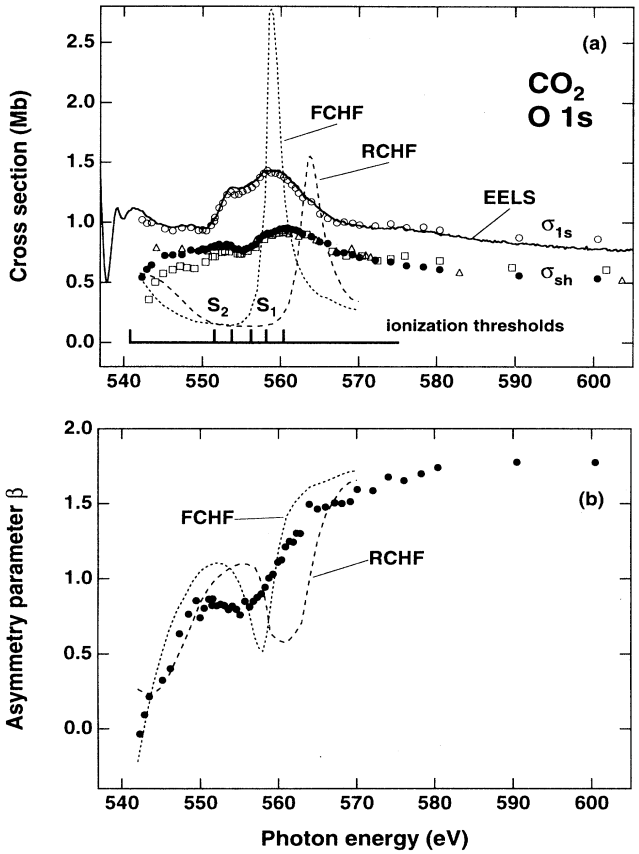

FIG. 3. (a) O 1s single-hole σ_{SH}(O) and total σ_{1s}(O) ionization cross section for CO_2. Three sets of measured data are shown for the single-hole cross section (△ and □) taken during two different measuring periods at the HE TGM monochromator ($\Delta E \sim 2.5$ eV) and (●) at the X1B monochromator ($\Delta E \sim 0.5$ eV). The total O 1s Auger intensity (○) (from X1B), which is proportional to the total O 1s cross section σ_{1s}(O), is compared to absolute EELS measurements (full line) [46]. The O 1s ionization threshold and the experimental thresholds [35] of the lowest shake-up satellites are indicated by bars below the curves. Also shown are calculations from McKoy and coworkers at the FCHF [42] and the RCHF [43] levels. (b) Experimental O 1s asymmetry parameter β in comparison with FCHF [42] and RCHF [43] calculations.

difference also appears in the photoionization of N_2O [13], where 1s ionization of the central (nitrogen) atom leads, in the vicinity of the shape resonance, to a stronger feature in the cross section compared to 1s ionization of the terminal atoms. Obviously, in both molecules the resonant σ^* continuum state has a much better overlap with the core level of the central atom. On a photoelectron kinetic-energy scale, the positions of the $4\sigma_u^*$ shape resonance for C 1s and O 1s ionization (in the single-hole cross sections) are found at ~ 14 and ~ 20 eV, respectively, but with a relatively large uncertainty due to overlapping structure. Experimentally, the positions differ by about 6 eV, in good agreement with the RCHF calculations, which give a value of ~ 4 eV. In our previous work on N_2O [13], similar energy shifts were observed, but a closer inspection of the RCHF eigenphase sums indicated that the true kinetic-energy position of the shape resonance is identical for all of the core holes. The different kinetic energies found experimentally were explained by the notion that the localized core holes probe different spatial parts of the resonant continuum wave function in the photoelectron matrix element. The same situation might be present for core-level photoionization of CO_2, but, unfortunately, no eigenphase sums were reported in the RCHF calculations [43].

The energy position of the C 1s $4\sigma_u^*$ shape resonance determined in the FCHF and RCHF calculations do not agree particularly well with the experimental results, but lie on each side of the measured maximum. Schirmer, Braunstein, and McKoy [49] have suggested that further calculations for CO C 1s photoionization at the RCHF level with the inclusion of target polarization would shift the theoretical curve to lower kinetic energy by 2–3 eV and bring the theory into better agreement with experiment. Presumably, the same effect would apply for both C 1s and O 1s ionization in CO_2. The major difference between the FCHF [42] and RCHF [43] calculations is the inclusion of electronic relaxation, which makes the effective molecular ion potential less attractive in the RCHF approach. This results in a shift of the shape resonance to higher energy, accompanied by a broadening and weakening of the resonance in going from the FCHF to the RCHF calculations. This energy shift is found to be very different for core photoionization of the central carbon atom and the terminal oxygen atoms in CO_2. For C 1s the resonance is shifted by approximately 11 eV, whereas for O 1s a smaller shift of about 4 eV occurs [compare Figs. 2(a) and 3(a)]. This, again, is completely analogous to our previous results for N_2O [13], indicating a much better screening of the core hole in the central atom.

The width and shape of the shape resonance represents a further discrepancy between theory and experiment, particularly for O 1s. The RCHF calculation shows a sharp profile, whereas our experimental results for the single-hole cross sections exhibit a broader feature. Three factors may be responsible for the broader resonance found in the experiment.

(i) McKoy and co-workers [42,43] have suggested that the resonance profile is characteristic of their HF approach using the full inversion symmetry for the core

ionized molecule, thus neglecting the potentially important effects of core hole localization. For example, included in their calculation of the $4\sigma_u^*$ shape resonance in CO_2 are the $l=3$, 5, and 7 partial waves and thus upon localization the continuum orbital will not have "pure" $k\sigma_u$ or $k\sigma_g$ symmetry, but will be a combination of both even and odd partial waves [43]. Hence, coupling to $l=4,6$ partial waves is expected. When included in the calculations, this would broaden the shape resonance. This effect has also been observed in the comparison of the calculated narrow N_2 $3\sigma_g \rightarrow \sigma_u^*$ ($l=3$) shape resonance [50] with the analogous but broader $5\sigma \rightarrow \sigma^*$ shape resonance in CO [51].

(ii) Calculations by Dehmer, Dill, and Wallace [52] on the $3\sigma_g \rightarrow \sigma_u^*$ shape resonance of N_2 have demonstrated that the resonance profile is extremely sensitive to the internuclear distance. Therefore, a proper averaging over the range of the ground-state vibrational motion is necessary, leading to a broadening of the profile.

(iii) As noted above, all experimental cross sections, i.e., $\sigma_{SH}(C)$, $\sigma_{1s}(C)$, $\sigma_{SH}(O)$, and $\sigma_{1s}(O)$, indicate strong additional structure in the region of the shape resonance, in contrast to the smooth profiles calculated by theory. This additional structure appears to substantially broaden the resonance and obscure the position of its maximum. It must be assigned to multielectron processes since there are no indications of such structure in the HF calculations. The presence of multielectron states is not surprising because the onsets for many shake-up satellites fall in this energy region [indicated in Figs. 2(a) and 3(a)] and each of these should be preceded by a Rydberg-type series of discrete doubly excited states. The latter may couple very differently to σ_{1s} or σ_{SH} leading to different intensities in each case. This aspect is discussed in more detail in the next section.

IV. THE INFLUENCE OF DOUBLY EXCITED STATES

In C 1s ionization of CO_2 we find good agreement between the form of $\sigma_{SH}(C)$ and $\sigma_{1s}(C)$ around the narrow feature at 303.5 eV, as well as for the two shoulders appearing at $\sim$311.5 and $\sim$314.5 eV [see Fig. 2(a)]. From the discussion above, we may safely assume that the structure at 303.5 eV, falling between the ionization threshold and the satellite onsets, is due to doubly excited states [19,24,53]. Until recently, however, the coupling of such states to the single-hole continuum was poorly understood [24]. It was believed that these discrete states would decay via a resonant Auger process [54], thus producing specific structure in the Auger electron spectrum (see Sec. VI below) but no photoelectrons. This is obviously in contradiction to the observation of Fig. 2(a), namely, that there is a strong intensity in the region of the doubly excited states in the *single-hole* cross section $\sigma_{SH}(C)$. In addition, we also find a strong perturbation in the angular distribution [Fig. 2(b)]: the β parameter changes by $\sim 0.4\,\beta$ units within 0.8 eV. Further, we note that the β-parameter curve is also distorted in the region of the shape resonance exactly where the two shoulders appear in the cross section. If the latter may also be assigned to multielectron states, then these too strongly interact with the single-hole continuum. We thus have a fast autoionization process into the 1s single-hole continuum giving additional intensity in this channel.

Multielectron effects in the O 1s ionization of CO_2 are less evident in the cross sections and also there are no clear effects discernible in the β parameter [Fig. 3(b)]. At the same time, however, there is a much greater redistribution of intensity. For example, the peak that may be assigned to discrete doubly excited states at 553 eV photon energy in $\sigma_{1s}(O)$ [Fig. 3(a)] [18,53] is reproduced in $\sigma_{SH}(O)$, albeit broader and with a reduced relative intensity. The same is true for the feature at 558 eV. Consequently, the overall intensity maximum in this energy region, consisting of multielectron states overlapping with the shape resonance, is shifted to higher energy in the single-hole cross section. Assuming that multielectron states may be reduced but not enhanced in the single-hole cross section, we can estimate that the maximum of the shape resonance is around 561 eV rather than $\sim$559 eV. Other weak structures at 548 and 575 eV in the total O 1s cross section $\sigma_{1s}(O)$ are barely evident in the single-hole cross section $\sigma_{SH}(O)$ and because their intensity is comparable to the scatter in the data, they cannot be identified unambiguously.

While the interpretation of structures below the onset of shake-up satellites in terms of doubly excited states is clear, the situation at higher energy is much more complicated because of the many discrete and continuum multielectron states. In addition to discrete multielectron resonances, the satellite cross section (possibly including the effects of resonances in some of these channels) could add structure to the total 1s cross section. A simple device that can be used to highlight these effects is to plot the difference between the $1s^{-1}$ single-hole and partial cross sections. This is illustrated in Figs. 4(a) and 4(b) for the case of C 1s and O 1s photoionization of CO_2, respectively. The difference curves $\sigma_{1s}(C)-\sigma_{SH}(C)$ and $\sigma_{1s}(O)-\sigma_{SH}(O)$ represent the sum of all shake-up and shake-off satellites together with other discrete multielectron channels that directly decay by an Auger process and do not produce photoelectrons. For high energies, decay via discrete multielectron channels are negligible, whereas below the lowest shake-up thresholds (see Fig. 4), they are the only explanation for a discrepancy between the total and single-hole cross section. The strong double-excitation feature at 303.5 eV in the C 1s cross section, for example, is clearly visible in the difference curve, indicating that only a fraction of these states produce photoelectrons.

The most prominent feature in the difference curves for both C 1s and O 1s ionization is a strong maximum in the region of the shake-up satellite onsets. Unfortunately, it is difficult to measure all satellite intensities down to virtually 0 eV kinetic energy in order to subtract this component and thus determine the remaining contribution from other multielectron channels. In the case of C 1s, however, an estimate of the satellite cross sections at low energies (see Sec. VI) shows that they could account for most of the difference in cross section. By chance, this broad intensity enhancement in some of the satellite

channels falls exactly on the shape resonance for C 1s, thus giving a nearly identical overall profile for σ_{1s}(C) and σ_{SH}(C). For O 1s, however, the shape resonance appears at slightly higher energy, giving rise to very different profiles and an apparent shift of the resonance position, as noted above.

For O 1s there is a steep increase in the cross section difference [Fig. 4(b)] at very low energy, which could indicate the presence of a discrete multielectron state having little interaction with the single-hole continuum. This is interesting since the enhancement in the total cross section just above the O 1s photoionization threshold has been assigned to the $5\sigma_g^*$ shape resonance [18,53], in agreement with the broad enhancement found in the RCHF calculation [43] [Fig. 3(a)]. We also note that the C 1s cross sections still seem to differ significantly at low energies (i.e., the difference does not go to zero at threshold), indicating the presence of other unresolved multielectron states. However, at these low energies the background subtraction is difficult, the errors in our spectrometer transmission are largest and the scaling of the single-hole cross sections critical. Therefore, further experimental and theoretical studies are necessary to investigate this point.

Our results for O 1s and C 1s photoionization of CO_2 clearly show that multielectron excitations are very prominent in the single-hole cross sections. The latter can therefore not be employed for identifying structures in the absorption spectrum as shape resonances or double excitations [55]. In particular, they cannot be used to recover the "one-electron" profile of a shape resonance. Similar effects have been recently observed for CO [23,24], C_6H_6 [56], and CS_2 [57]. Only in favorable cases, when there are substantial differences in the intensities between the total and single-hole cross section, it may be possible to distinguish between single- and multiple-electron effects.

V. SATELLITES

We turn now to the photon energy dependence of the strongest C 1s satellites of CO_2 from kinetic energies of $\sim 5-\sim 100$ eV, thus encompassing the near threshold and sudden limit conditions. (The shake-up satellites in O 1s could not be investigated in detail due to strong overlap of various satellite lines within a narrow energy region. This would have required a high resolution and consequently, at the present time, a prohibitive amount of measurement time for good statistics.) In Fig. 5, C 1s spectra (measured at the HE TGM) are shown for the photon energy range 319.8–402.6 eV. The satellite peaks are assigned by comparison with theory as well as utilizing characteristic intensity and angular distribution behavior evident from the data themselves. Angonoa and Schirm-

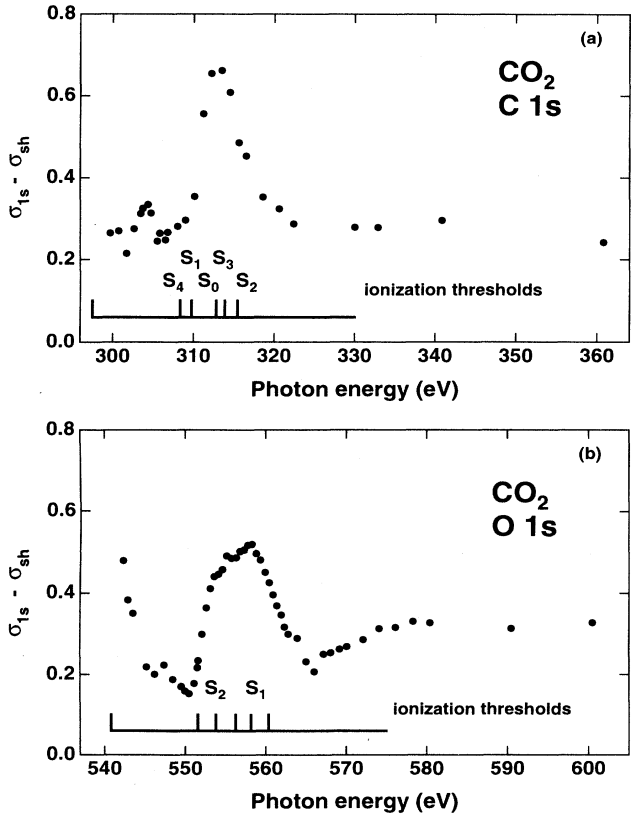

FIG. 4. Difference between the total and the single-hole cross sections as a function of photon energy for (a) C 1s and (b) O 1s.

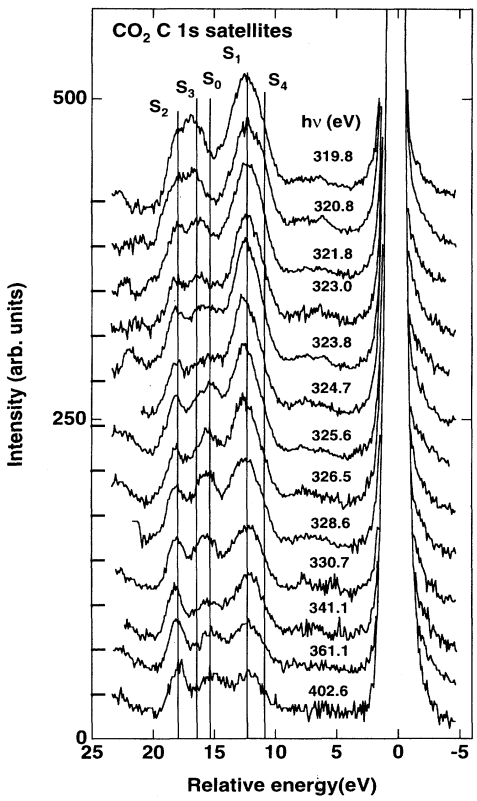

FIG. 5. C 1s satellite spectra taken on the HE TGM at BESSY. The spectra have been normalized relative to the C 1s main line and recorded with a combined CMA-monochromator resolution of 1.2 eV. A smooth secondary-electron background has been subtracted.

er [36] have carried out extensive ADC(4) calculations that clearly indicate that the lowest-lying satellites appearing at $E_{rel}=12.3$ and 15.3 eV can be assigned to triplet (S_1) and singlet (S_0) coupled $2\sigma_g^{-1}1\pi_u^{-1}2\pi_u^1$ configurations, respectively. Similarly, the comparatively strong line (S_2) appearing at $E_{rel}=18.0$ eV is assigned to the $2\sigma_g^{-1}3\sigma_g^{-1}n\sigma_g^1$ excitation, with a strong admixture from a $2\sigma_g^{-1}1\pi_u^{-1}2\pi_u^1$ configuration. Additionally, the three satellites S_1, S_0, and S_2 show mixing with double excitations of the form $2\sigma_g^{-1}1\pi_g^{-2}2\pi_u^2$ and $2\sigma_g^{-1}1\pi_u^{-2}2\pi_u^2$; these are particularly strong for S_0 and S_2. Since all three satellites belong to the $^2\Sigma_g^+$ configuration, they will be present at high photon energies with significant intensity, as is evidenced in the spectrum taken at a photon energy of 402.6 eV and in the high-resolution x-ray photoemission spectroscopy (XPS) Al $K\alpha$ spectrum [35].

The satellite spectrum is different below energies of $\sim$402 eV and dramatic changes occur as the energy decreases below $\sim$325 eV. More specifically, as can be seen from Fig. 5, the relative intensity of S_2 remains constant, while there is an increase in intensity of S_0 and S_1, compared to that of the main line, down to a photon energy of $\sim$325 eV. Below this energy there is a strong enhancement of S_1, while S_0 vanishes within a very narrow energy range (320.8 eV $<h\nu<$ 325.6 eV). This behavior is comparable to that observed for the singlet and triplet coupled C 1s π-π^* $^2\Sigma^+$ satellites of CO, which show a similar energy dependence [23,25,26,32], although in the case of CO C 1s, these intensity variations occur over a much larger kinetic-energy range. The similarity to CO suggests that the intensity behavior of S_1 and S_0 can be interpreted as being due to constructive and destructive interference, respectively, of the direct and conjugate part of the transition moment [28]. The lack of calculations, however, precludes a confirmation of this interpretation.

Below $\sim$325 eV photon energy, an additional satellite peak is apparent between S_0 and S_2, the intensity of which is enhanced as the satellite threshold is approached. We denote this satellite as S_3 with an energy of 16.2 eV relative to the C 1s main line. A closer inspection of the data from the HE TGM also shows that S_1 becomes broader towards lower kinetic energies. Measurements at higher resolution on the X1B monochromator ($\Delta E=0.2$ eV) revealed that the satellite band, denoted as S_1, actually consists of at least two components, as can be seen in Fig. 6. These satellites are located very close together. The additional component (denoted as S_4), at an energy of 10.9 eV relative to the main line, shows an intensity behavior similar to that of S_3. Since S_3 and S_4 do not appear in the XPS [35] spectrum they must be assigned to a conjugate mechanism associated with a different final state symmetry, presumably $2\sigma_g^{-1}1\pi_u^{-1}2\pi_u^1$ states with Σ_g^- or Δ_g symmetry.

In Fig. 7 the experimental cross section and asymmetry parameters of the satellite lines are shown. These have been obtained by using some simplifying assumptions in the line-shape analysis: (i) the satellite band S_3 is assumed to consist of only one (broad) line located at $E_{rel}=16.2\pm0.2$ eV; (ii) within the critical energy range of 318 eV $<h\nu<$ 325 eV both the position and width of S_0,

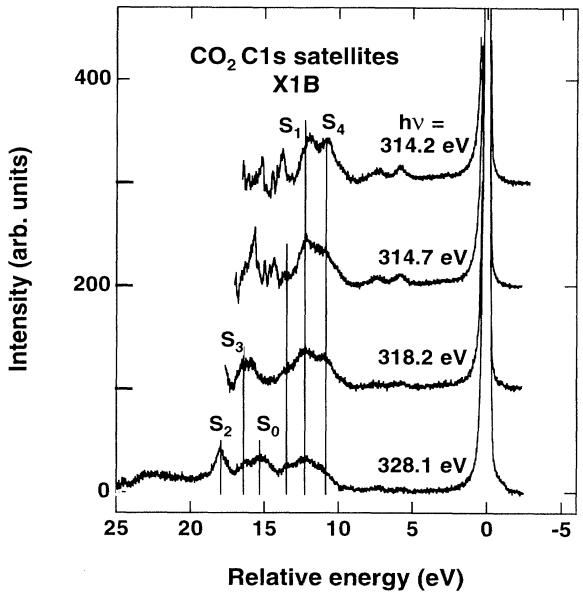

FIG. 6. High-resolution C 1s satellite spectra taken on the X1B undulator beam line at the NSLS, Brookhaven. Several extra satellites are revealed. The spectra have been normalized relative to the C 1s main line and have been recorded with a combined CMA-monochromator resolution of $\sim$0.2 eV.

S_2, and S_3 are kept fixed; and (iii) a (fixed) linear combination of Gaussian and Lorentzian line shapes approximates the experimental line profile. In the fit procedure $S_1$and S_4 could not be distinguished due to poor resolution on the HE TGM. The position and width of S_1+S_4 were allowed to vary in the fit.

It is evident that for photon energies above 340 eV, the relative cross sections of the three main satellites approach a constant value in agreement with spectra taken in the sudden limit. Below this energy, S_0 exhibits a maximum in intensity at $\sim$328 eV that falls dramatically for energies $h\nu<325$ eV. In contrast, a strong enhancement of intensity can be observed for S_1+S_4 and S_3 for energies below 325 eV [Fig. 7(a)]. The maximum in S_0 occurs at approximately the same kinetic energy as the maximum in the single-hole shape resonance and could be indicative of a shape resonance in this satellite channel. In addition, we also observe a slight broadening of S_1+S_4 accompanied by a small shift of the peak maximum towards lower binding energy. This broadening and shift is due to the enhancement in intensity of S_4, which can be clearly observed in the higher-resolved spectra (Fig. 6). Although it was not possible to evaluate satellite intensities at kinetic energies lower than about 5 eV, we can nevertheless obtain some measure of the S_1 and S_4 satellite intensity in the 0–5 eV energy region from Fig. 4(a). Clearly there is virtually no satellite intensity below 310 eV photon energy, i.e., S_1 and S_4 must decrease nearly to zero intensity just above their thresholds at 309.8 and 308.4 eV, respectively. However, S_1+S_4 has probably not reached its maximum in Fig. 7(a): the data in Fig. 4(a) indicate a peak intensity of

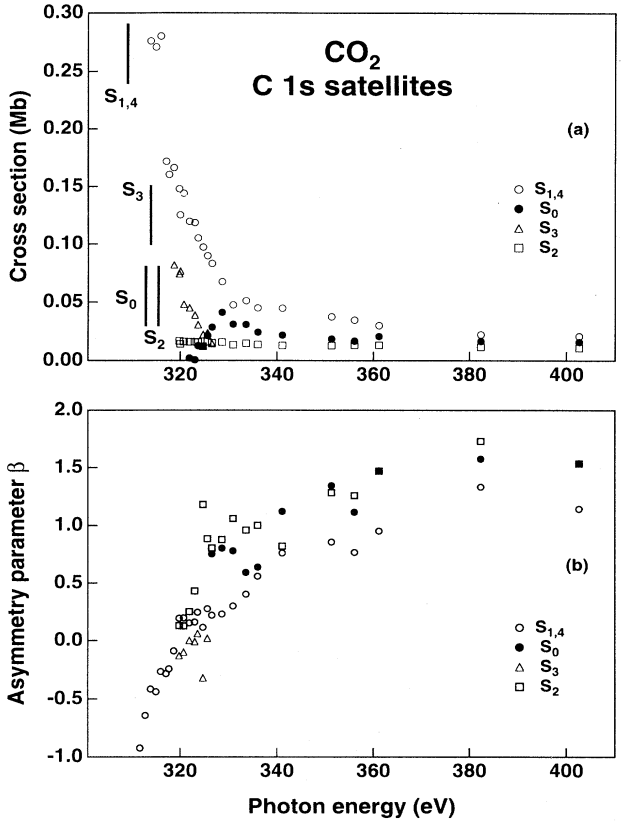

FIG. 7. (a) Partial cross sections for the C 1s satellites of CO_2: ●, S_0; ○, S_1+S_4; □, S_2; and △, S_3. (b) The corresponding asymmetry parameters for the satellites. The vertical bars indicate the satellite thresholds.

~0.4 Mb, producing a very narrow and intense feature in the partial cross section. (Note that part of this cross section could also be due to autoionization of a discrete multielectron state.) A comparable situation holds for the corresponding C 1s triplet coupled S_1 satellite of CO near threshold, which consists of at least three components [23,30,32].

The results for the asymmetry parameters for the CO_2 C 1s satellites are shown in Fig. 7(b). Although limited by the scatter in the data, there is some evidence for oscillatory behavior in the three main satellites S_1+S_4, S_0, and S_2 similar to that in the C 1s main line, suggesting the influence of the $4\sigma_u^*$ shape resonance on these channels. For S_1 and S_0 this interpretation is supported by the cross-section enhancement in this energy region, although this behavior may also be due to an interference effect in the transition moment as discussed above. For S_2 we do not observe a cross-section enhancement, which might indicate the existence of the shape resonance in this channel. Note that the S_4 conjugate satellite strongly affects the asymmetry parameter of S_1+S_4, which becomes negative near threshold. The other conjugate satellite S_3 shows an isotropic angular distribution.

In addition to the conjugate shake-up satellites S_3 and S_4, the higher-resolved spectra (Fig. 6) confirm the presence of two further peaks at energies of 5.8 and 7.3 eV relative to the main line. These gain intensity towards threshold, as can also be seen in Fig. 5. A possible explanation might be conjugate shake-up transitions to give $2\sigma_g^{-1}1\pi_g^{-1}2\pi_u^1$ configurations. These states are not accessible via a direct shake-up process and therefore would not be visible in the XPS spectrum at 1486.6 eV [35]. Based on the orbital energy diagram of the neutral molecule, they should appear at lower binding energies than the strong $2\sigma_g^{-1}1\pi_u^{-1}2\pi_u^1$ satellites. From the spatial properties of the $1\pi_g$ orbital, which is localized on the oxygen atoms, and the $2\pi_u$ orbital, which is centered around the carbon atom [58], a $2\sigma_g^{-1}1\pi_g^{-1}2\pi_u^1$ excitation should lead to strong charge transfer towards the carbon atom. This would induce an additional electronic screening of the C 1s hole, thus reducing the shake-up energies. However, better statistics and extended calculations are required to check this explanation.

Due to the high-energy resolution and the lower background from secondary electrons on the X1B monochromator, the spectra taken at 314.7 and 314.2 eV photon energy (Fig. 6) indicate, in addition to the satellites, narrow peaks at fixed kinetic energies. These features are due to secondary Auger transitions from highly excited valence states following the first Auger decay of the core hole. The spectra shown in Fig. 6 highlight the problem of assignment in this low-kinetic-energy region (i.e., near the onset of the satellite thresholds), where there is overlap of the Auger electrons with the satellite lines.

VI. RESONANT AUGER ELECTRON SPECTRA

In Sec. IV we showed that certain doubly excited states interact strongly with the 1s single-hole continuum, resulting in narrow features in the C 1s and O 1s single-hole cross sections at 303.5 and 553.0 eV, respectively. This interpretation is consistent with a mechanism by which these states preferentially autoionize into the 1s continuum followed by a normal Auger decay of the 1s hole state. This leaves behind a *doubly* charged molecular ion with two holes ($2h$) in the valence shell, as shown in Fig. 8(a). Besides this two-step mechanism, the doubly excited states may alternatively decay, but with a lower probability, via a single-step resonant Auger process producing *singly* charged final states. Neglecting shake-up and shake-off processes, these singly charged final states can be $3h$-$2e$, $2h$-$1e$, or $1h$ states, depending on whether the two excited electrons both remain as spectator electrons, whether one of them remains, or whether both participate in the decay process, respectively. These three types of decay mechanisms are schematically shown in Figs. 8(b)–8(d).

Similar processes leading to the same singly charged final states occur also in the decay of $1s^{-1}np^1$ states where the core electron is excited to an unoccupied bound molecular or Rydberg orbital, as shown in Fig. 8(e). The decay spectrum of the $1s^{-1}2\pi_u^1(\pi^*)$ resonance in CO_2 has already been discussed in detail by Thomas [29]. It contains a significant contribution from "participator transitions" leading to $1h$ final states. The main contribution, however, comes from "spectator transi-

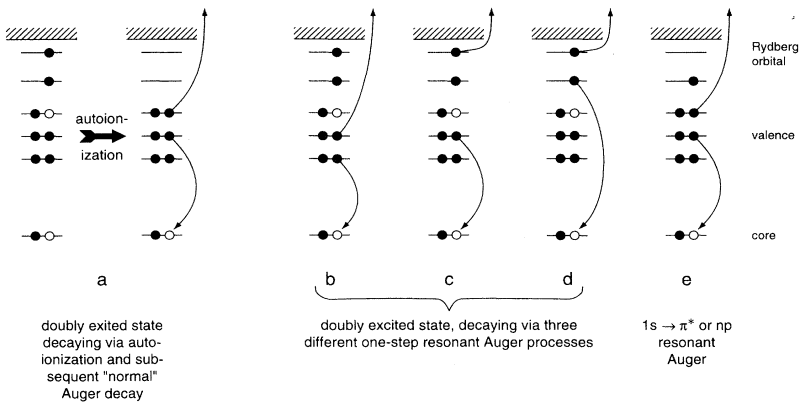

FIG. 8. Schematic diagram of the different Auger decay processes. (a) Doubly excited state decaying via autoionization and a "normal" Auger decay. Doubly excited states with (b) two spectator electrons, (c) one spectator electron, or (d) both excited electrons participating in the decay process. (e) $1s \rightarrow \pi^*$ or *np* resonant Auger decay.

tions" with $2h$-$1e$ final states [indicated in Fig. 8(e)], leading essentially to a shift of the normal Auger spectrum (with $2h$ final states) to higher kinetic energy, due to the screening by the spectator electron [29,59,60]. Note that the same $2h$-$1e$ final states may be accessible via the decay of a singly excited $1s^{-1}np^1$ intermediate state as well as in that of a doubly excited $1s^{-1}v_1^{-1}v_2^1np^1$ state, as indicated in Figs. 8(e) and 8(c). In fact, the doubly excited states can be regarded as shake-up satellites of the $1s^{-1}np^1$ states, suggesting that satellites of the $1s^{-1}2\pi_u^1$ transition might have particularly high intensity. The singly charged $1h$, $2h$-$1e$, etc., final states are also well known from valence photoelectron spectra using uv radiation where they appear as main lines and shake-up satellites, respectively [61]. However, the different initial states and selection rules for photoelectron spectroscopy and resonant Auger decay give rise to very different relative intensities.

If a significant fraction of the doubly excited states decay in a direct, resonant Auger process, one should, in principle, be able to observe additional structure superimposed on the normal Auger spectrum. In order to verify our interpretation and to obtain a more detailed understanding of the processes involved, we have measured Auger spectra on the strong double excitation structure at 303.5 eV, as well as on the (singly excited) bound resonances below the C $1s$ ionization threshold. These spectra will be compared with the normal Auger spectrum, measured in the continuum at energies well above the discrete resonances and with the valence level photoelectron spectrum.

The nonresonant and the resonant C $1s$ Auger spectra measured at photon energies of 306 and 303.5 eV, respectively, are shown in Figs. 9(a) and 9(b), together with the decay spectra of the three discrete resonances [at 294.9 eV, corresponding to the C $1s \rightarrow 3p(\sigma_u)$, C $1s \rightarrow 3p(\pi_u)$, and C $1s \rightarrow 4s(\sigma_g)$ transitions; at excitation energies of 292.7 eV, i.e., the C $1s \rightarrow 3s(\sigma_g)$ transition, and at 290.7 eV, i.e., the C $1s \rightarrow 2\pi_u(\pi^*)$ transition] below the C $1s$ ionization threshold [Figs. 9(c)–9(e)]. Also shown in the photoelectron spectrum measured at a photon energy of 100 eV [Fig. 9(f), taken from [61]]. All spectra are shown on a binding-energy scale, defined as the difference between the photon energy used for the excitation and the electron kinetic energy. On this scale, identical final states in the resonant spectra line up at the same energy,

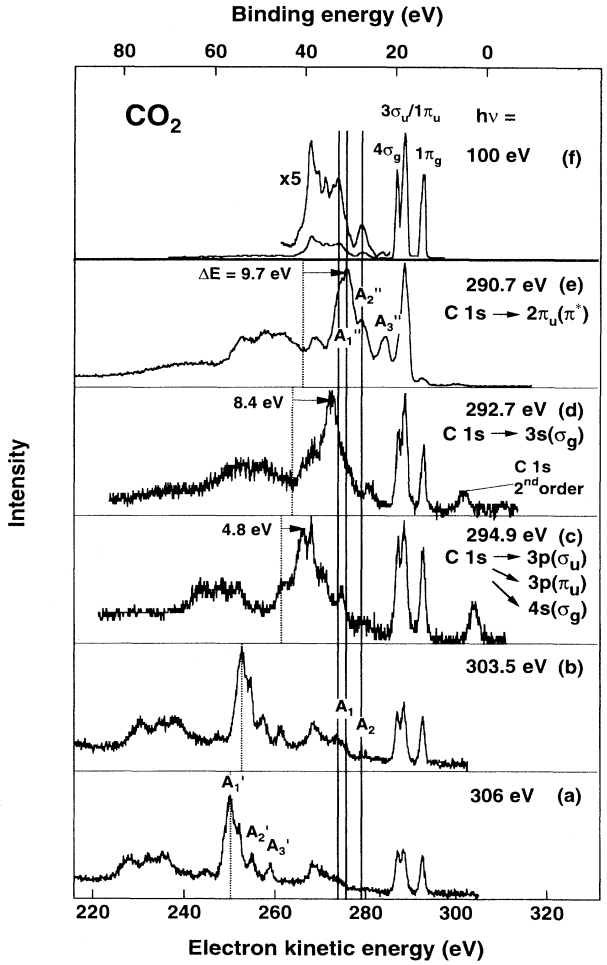

FIG. 9. C $1s$ Auger and valence electron spectra measured (a) at a photon energy of 306 eV in the continuum; (b) at 303.5 eV on the double excitation; (c) at 294.9 eV on the C $1s \rightarrow 3p(\sigma_u)$, C $1s \rightarrow 3p(\pi_u)$, and C $1s \rightarrow 4s(\sigma_g)$ transitions; (d) at 292.7 on the C $1s \rightarrow 3s(\sigma_g)$ transition; and (e) at 290.7 eV on the C $1s \rightarrow 2\pi_u(\pi^*)$ transition. (f) is the normal photoemission spectrum measured at a photon energy of 100 eV by Freund, Kossmann, and Schmidt [61]. All spectra are shown on a binding-energy scale (top). The kinetic-energy axis (bottom) only refers to spectrum (a) measured at 305 eV.

thus aiding in the assignment of unknown structures. This follows from simple energetic considerations (see also [59,60]): the kinetic energy of an Auger electron E_A is given by the difference between the energy of the excited state $E_{\rm exc}$ and the final state energy E_f. For discrete resonances, $E_{\rm exc}$ is identical with the energy of the exciting photon; for the normal Auger transition (with the core electron ionized) it is equal to the binding energy of the core electron. For identical final states populated from different discrete (resonant) intermediate states, such as those depicted in Figs. 8(c) and 8(e), the energy difference between the intermediate states $E_{\rm exc,1}-E_{\rm exc,2}$ is the same as that of the Auger electrons $E_{A,1}-E_{A,2}$, hence the binding energies $E_{\rm exc,1}-E_{A,1}$ and $E_{\rm exc,2}-E_{A,2}$ are the same.

All spectra shown in Fig. 9 include the photoelectron lines of the outer $1\pi_g$, $1\pi_u$-$3\sigma_u$, and $4\sigma_g$ valence electrons at 17, ~19, and 21 eV binding energy, respectively. (Due to the low-energy resolution of ~2 eV, we cannot resolve the $1\pi_u$ and $3\sigma_u$ photoelectron lines expected at 17.3 and 18.1 eV.) Some of these lines are enhanced in the spectra measured on the resonances below the C 1s threshold [Figs. 9(c)–9(e)] compared to the spectrum measured at 306 eV photon energy [Fig. 9(a)], which contains no significant contribution from a discrete resonant state. The additional intensity is due to participator Auger decay processes whose contribution to particular 1h states depend on the symmetry and overlap of the orbitals involved. For example, in the decay of the C $1s\rightarrow 2\pi_u(\pi^*)$ resonance [Fig. 9(e)], a strong enhancement of the $1\pi_u^{-1}$ final state is observed, but only a relatively small increase in intensity from the $3\sigma_u^{-1}$, $4\sigma_g^{-1}$, and $1\pi_g^{-1}$ final states. Theory, in contrast, predicts little intensity in the $1\pi_u^{-1}$ final state and a $4\sigma_g^{-1}$ contribution stronger than that of the $1\pi_u^{-1}$ state [29]. The other resonances at 292.7 and 294.9 eV [Figs. 9(d) and 9(c)] lead to an enhancement of all three outer valence lines, although with slightly different weighting. The resonance at 292.7 eV has been assigned to a transition of a C 1s electron into a $3s(\sigma_g)$ state, that at 294.9 eV to a transition into a mixture of $3p(\sigma_u)$, $3p(\pi_u)$, and $4s(\sigma_g)$ states, which could not be resolved with our photon energy bandwidth of ~1 eV. A careful comparison of the spectrum measured on the resonance at 303.5 eV [Fig. 9(b)] with the spectrum measured in the continuum at 306 eV [Fig. 9(a)] also reveals a small enhancement of the 1h states, in particular of the $1\pi_u$-$3\sigma_u$ line at ~19 eV binding energy, indicating the presence of decay processes in which both excited electrons of the doubly excited state participate.

At higher binding energies, between 22 and 45 eV, a multitude of states is observed in the uv photoelectron spectrum [Fig. 9(f)] and in the spectra measured at 306 and 303.5 eV photon energy [Figs. 9(a) and 9(b)]. This inner valence region is characterized by a complicated mixture of $2\sigma_u^{-1}$ and $3\sigma_g^{-1}$ 1h states and various 2h-1e states with different degrees of 1h admixtures [29,61–63]. In this binding-energy region we also find the most intense features of the resonant Auger spectra measured on the singly excited bound states below the C 1s ionization threshold [Figs. 9(c)–9(e)]. In principle, these features can therefore be assigned to states observed in the uv photoemission spectrum, although this is difficult in practice due to the complexities of the spectrum.

Another approach for the assignment is a comparison with the normal Auger spectrum [Fig. 9(a)]. It is well known (and also obvious from Fig. 9) that the resonant spectra are very similar to the normal Auger spectrum, except for some intensity redistribution and, most notably, a shift to higher kinetic energy due to the screening effect of the excited electron remaining as a spectator. The shift, i.e., the difference in binding energy between the 2h and the 2h-1e final states, is indicated for the strongest feature A_1' in Fig. 9 and amounts to approximately 4.8, 8.4, and 9.7 eV for the spectra measured at 294.9, 292.7, and 290.7 eV [Figs. 9(c)–9(e)], respectively. While a detailed assignment of the most intense feature A_1' and its analog A_1'' in the resonant spectra in the binding-energy region between 30 and 40 eV is very difficult, there is agreement between different theoretical calculations as to the origin of the broad peaks A_2'' and A_3'' at binding energies of ~27.5 and ~23 eV, corresponding to structures A_2' and A_3' at 254.5 and 259 eV kinetic energy, respectively, in the normal Auger electron spectrum [Fig. 9(a)]. A_2' has been assigned to $1\pi_g^{-1}1\pi_u^{-1}$ and $3\sigma_u^{-1}1\pi_u^{-1}$ configurations [64,65], in agreement with calculations by Porwol *et al.* [62], who assign the corresponding feature in the resonant C $1s\rightarrow 2\pi_u(\pi^*)$ spectrum, A_2'' [Fig. 9(e)], to $1\pi_g^{-1}1\pi_u^{-1}2\pi_u$ and $3\sigma_u^{-1}1\pi_u^{-1}2\pi_u$ states. A_3' has been assigned to a $1\pi_g^{-2}$ state [64,65], also in agreement with Porwol *et al.* [62], who calculated a $1\pi_g^{-2}2\pi_u$ configuration for the corresponding structure A_3''.

Based on the discussion of the decay of the singly excited resonances below the C 1s ionization threshold [Figs. 9(c)–9(e)] we can now try to interpret the spectrum measured on the double-excitation resonance at 303.5 eV photon energy [Fig. 9(b)]. There is no dramatic difference between this spectrum and the normal Auger spectrum [Fig. 9(a)], in agreement with our finding that the resonance at 303.5 eV is nearly as intense in the C 1s single-hole partial cross section as it is in the total C 1s cross section [Fig. 2(a)]. A more detailed examination, however, reveals two additional very weak enhancements of intensity at ~32 eV (A_1) and at ~27 eV (A_2) binding energy as well as a minor intensity change below 260 eV kinetic energy (corresponding to binding energies above 43 eV). Although considerably weaker than the analogous features observed previously in CO [24], the appearance of the peaks A_1 and A_2 confirms the multielectron nature of the narrow resonance observed in the total and the single-hole cross section at 303.5 eV.

The low binding energies of A_1 and A_2, falling in the energy region of the inner valence states discussed above, suggest that these features are related to 2h-1e final states such as that indicated in Fig. 8(c), where one of the two excited electrons participates in the decay process and the other remains as a spectator. A more specific assignment may be achieved by a comparison of features A_1 and A_2 with structure at the same binding energies in the

photoelectron spectrum [Fig. 9(f)] and in the other resonant spectra [Figs. 9(c) and 9(d)]. The strongest feature A_1 has exactly the same binding energy as the strongest Auger structure A_1'' in the C $1s \rightarrow 2\pi_u(\pi^*)$ decay spectrum [Fig. 9(e)]. This suggests that the Auger decay of the doubly excited states leads predominantly to $2h$-$1e$ final states with one electron excited in the $2\pi_u$ orbital (although the calculations of Porwol *et al.* [62] have shown that strong correlations to other satellite configurations are also present). Such $2h$-$1e$ final states are in agreement with the assumption that the origin of the doubly excited states at 303.5 eV photon energy is a C $1s \rightarrow 2\pi_u$ excitation accompanied by a shake-up transition of an outer valence electron, e.g., $1\pi_u$ to a Rydberg orbital. The fastest Auger decay route of these states seems to be one in which the Rydberg electron participates in the decay process while the $2\pi_u$ electron remains as a spectator. The opposite case, i.e., the $2\pi_u$ electron leaving and the Rydberg electron remaining, does not appear to be important because we do not observe significant additional structure [in Fig. 9(b)] at binding energies where the Rydberg-excited decay spectra [Figs. 9(c) and 9(d)] have their highest intensity. This also suggests that the relatively broad structure A_1 is probably not related to the narrow and much less intense line at the same binding energy present in the resonant spectrum measured at 294.9 eV [Fig. 9(c)].

The other additional structure in the resonant Auger electron spectrum at 303.5 eV photon energy A_2 can be associated with the feature A_2'' in the C $1s \rightarrow 2\pi_u(\pi^*)$ decay spectrum [Fig. 9(e)] and corresponding peaks in the uv photoemission spectrum [Fig. 9(f)] and the normal Auger electron spectrum [A_2' in Fig. 9(a)]. According to the theoretical calculations for A_2' and A_2'' [62,64,65], A_2 is therefore assigned to $1\pi_g^{-1}1\pi_u^{-1}2\pi_u$ and $3\sigma_u^{-1}1\pi_u^{-1}2\pi_u$ states where again, as for A_1, the $2\pi_u$ electron remains as a spectator.

There is no additional structure visible in Fig. 9(b) at $\sim$23 eV binding energy where one could expect intensity from a $1\pi_g^{-2}2\pi_u$ configuration [62,64,65], corresponding to A_3' and A_3'' in the spectra of Figs. 9(a) and 9(e), respectively. Apart from the fact that this channel is relatively weak in all spectra due to the small overlap of the C $1s$ with the $1\pi_g$ orbital [58], a primary excitation of the $1\pi_g$ orbital would be necessary to make a $1\pi_g^{-2}2\pi_u$ final state possible. The missing structure A_3 is therefore consistent with the assignment of A_2 as $1\pi_g^{-1}1\pi_u^{-1}2\pi_u^1$ and $3\sigma_u^{-1}1\pi_u^{-1}2\pi_u^1$ final states, which could result from the decay of doubly excited states of the type $1s^{-1}1\pi_u^{-1}2\pi_u^1R^1$.

Similar experiments for O $1s$ excitation of CO_2 were also undertaken, but due to the high kinetic energies we were unable to measure O $1s$ Auger spectra with sufficiently high energy resolution and signal-to-noise ratio. Dramatic effects, however, such as those observed for C $1s$ excitation of CO [24], can be excluded.

VII. SUMMARY

We have measured C $1s$ and O $1s$ partial cross sections and angular distributions of CO_2 with high precision near the photoionization threshold. This region covers both the $4\sigma_u^*$ shape resonance and the less intense structure at lower photon energy, which is due to multielectron excitations. The shape resonance is well reproduced in the $1s$ single-hole cross sections, but strong site-specific effects manifest themselves in the energy and strength of the shape resonances as well as in the oscillatory behavior of the angular distribution in this energy region.

Partial cross sections and angular distributions have also been measured for the first group of strong shake-up satellites in the C $1s$ photoelectron spectrum. Similar to the C $1s$ ionization of CO, we find a strong enhancement of the triplet-coupled π-π^* satellite (S_1) near threshold while the singlet-coupled satellite (S_0) disappears. A third satellite (S_2) has a constant cross section. At low photon energies, additional satellites at 5.8, 7.3, 10.9 (S_4), and 16.2 eV (S_3) are observed that are attributed to conjugate shake-up. Both S_3 and S_4 show a resonant enhancement towards threshold. Their angular distribution, however, is very different: while it is isotropic for S_3, it becomes negative for S_4 at low energies.

A striking feature of the present investigation is the presence of fine structure in the $1s$ single-hole cross sections σ_{SH} due to multielectron excitations: virtually all spectral details in the total $1s$ cross sections σ_{1s} are also present in σ_{SH}, implying that multielectron excitations can couple strongly to the underlying $1s$ continuum. The coupling strength, however, can obviously be quite different and may lead to a strong intensity redistribution in σ_{SH} as indicated by the O $1s$ data. Consequently, it is generally difficult to separate the different contributions and, in particular, to isolate the shape resonance profile. Thus a more quantitative comparison with theory is only possible if multielectron effects are taken into account in the calculations. First attempts to develop a computational approach to include relaxation, multiconfiguration, and multichannel effects have recently been made by Bandarage and Lucchese and applied to the C $1s$ ionization of CO [66].

The decay dynamics of the double-excitation feature at 303.5 eV in the C $1s$ cross section of CO_2 have been characterized by Auger spectroscopy. Small additional features in the resonant Auger spectrum could be identified by comparing, on an electron binding-energy scale, with the uv photoelectron spectrum, the normal Auger spectrum and resonant Auger spectra measured on single-hole bound resonances. The results agree with the assignment of the double excitation as $1s^{-1}1\pi_u^{-1}2\pi_u^1R^1$.

ACKNOWLEDGMENTS

We thank V. McKoy, J. Schirmer, and D. Nordfors for communicating unpublished data. We acknowledge financial support from the German Federal Ministry of Research and Technology under Contract No. 05 5EBFXB 2/TP6. The National Synchrotron Light Source at Brookhaven National Laboratory is supported by the U.S. Department of Energy under Contract No. DE-AC02-76CH00016.

[1] See, for example, J. L. Dehmer, A. C. Parr, and S. H. Southworth, in *Handbook on Synchrotron Radiation,* edited by G. V. Marr (North-Holland, Amsterdam, 1986), Vol. II, pp. 241–353.
[2] D. L. Lynch and V. McKoy, Phys. Rev. A **30**, 1561 (1984).
[3] Y. Ma, C. T. Chen, G. Meigs, K. Randall, and F. Sette, Phys. Rev. A **44**, 1848 (1991).
[4] C. T. Chen, Y. Ma, and F. Sette, Phys. Rev. A **40**, 6737 (1989).
[5] K. J. Randall, J. Feldhaus, W. Erlebach, A. M. Bradshaw, W. Eberhardt, Z. Xu, Y. Ma, and P. D. Johnson, Rev. Sci. Instrum. **63**, 1367 (1992).
[6] K. J. Randall, A. L. D. Kilcoyne, H.-M. Köppe, J. Feldhaus, A. M. Bradshaw, J.-E. Rubensson, W. Eberhardt, Z. Xu, P. D. Johnson, and Y. Ma, Phys. Rev. Lett. **71**, 1156 (1993).
[7] U. Gelius, J. Electron Spectrosc. Relat. Phenom. **5**, 985 (1974); C. J. Allan, U. Gelius, D. A. Allison, G. Johansson, H. Siegbahn, and K. Siegbahn, *ibid.* **1**, 131 (1972).
[8] R. L. Martin and D. A. Shirley, J. Chem. Phys. **64**, 3685 (1976).
[9] H. W. Meldner and D. D. Perez, Phys. Rev. A **4**, 1388 (1971).
[10] T. Åberg, Phys. Rev. **156**, 35 (1967); Ann. Acad. Sci. Fenn. A VI **308**, 1 (1969); Phys. Rev. A **2**, 1726 (1970).
[11] L. Asplund, U. Gelius, S. Hedman, K. Helenelund, K. Siegbahn, and P. E. M. Siegbahn, J. Phys. B **18**, 1569 (1985).
[12] F. A. Gianturco, M. Guidotti, and U. Lamanna, J. Chem. Phys. **57**, 840 (1972).
[13] M. Schmidbauer, A. L. D. Kilcoyne, K. J. Randall, J. Feldhaus, A. M. Bradshaw, M. Braunstein, and V. McKoy, J. Chem. Phys. **94**, 5299 (1991).
[14] A. L. D. Kilcoyne, M. Schmidbauer, A. Koch, K. J. Randall, and J. Feldhaus, J. Chem. Phys. **98**, 6735 (1993).
[15] T. A. Carlson, P. R. Keller, J. W. Taylor, T. Whitley, and F. A. Grimm, J. Chem. Phys. **79**, 97 (1983).
[16] M. Braunstein and V. McKoy, J. Chem. Phys. **87**, 224 (1987).
[17] N. Padial, G. Csanak, B. V. McKoy, and P. W. Langhoff, Phys. Rev. A **23**, 218 (1981).
[18] W. R. Daasch, E. R. Davidson, and A. U. Hazi, J. Chem. Phys. **76**, 6031 (1982).
[19] M. Domke, C. Xue, A. Puschmann, T. Mandel, E. Hudson, D. A. Shirley, and G. Kaindl, Chem. Phys. Lett. **173**, 122 (1990).
[20] G. R. Wight, C. E. Brion, and M. J. Van Der Wiel, J. Electron Spectrosc. Relat. Phenom. **1**, 457 (1972).
[21] A. P. Hitchcock and C. E. Brion, J. Electron Spectrosc. Relat. Phenom. **10**, 317 (1977).
[22] G. R. Wight and C. E. Brion, J. Electron Spectrosc. Relat. Phenom. **4**, 191 (1974); **4**, 313 (1974).
[23] H.-M. Köppe, A. L. D. Kilcoyne, J. Feldhaus, and A. M. Bradshaw (unpublished).
[24] M. Schmidbauer, A. L. D. Kilcoyne, H.-M. Köppe, J. Feldhaus, and A. M. Bradshaw, Chem. Phys. Lett. **199**, 119 (1992).
[25] L. Ungier and T. D. Thomas, Phys. Rev. Lett. **53**, 435 (1984).
[26] A. Reimer, J. Schirmer, J. Feldhaus, A. M. Bradshaw, U. Becker, H. G. Kerkhoff, B. Langer, D. Szostak, R. Wehlitz, and W. Braun, Phys. Rev. Lett. **57**, 1707 (1986).
[27] J. Feldhaus, A. Reimer, J. Schirmer, A. M. Bradshaw, U. Becker, H. G. Kerkhoff, B. Langer, D. Szostak, R. Wehlitz, and W. Braun, J. Phys. (Paris) Colloq. **48**, C9-773 (1987).
[28] J. Schirmer, M. Braunstein, and V. McKoy, Phys. Rev. A **44**, 5762 (1991).
[29] T. D. Thomas, Phys. Rev. Lett. **52**, 417 (1984).
[30] L. J. Medhurst, P. A. Heimann, M. R. F. Siggel, D. A. Shirley, C. T. Chen, Y. Ma, S. Modesti, and F. Sette, Chem. Phys. Lett. **193**, 493 (1992).
[31] L. J. Medhurst, T. A. Ferrett, P. A. Heimann, D. W. Lindle, S. H. Liu, and D. A. Shirley, J. Chem. Phys. **89**, 6096 (1988).
[32] T. Reich, P. A. Heimann, B. L. Petersen, E. Hudson, Z. Hussain, and D. A. Shirley, Phys. Rev. A **49**, 4570 (1994).
[33] M. O. Krause and C. D. Caldwell, Phys. Rev. Lett. **59**, 2736 (1987).
[34] B. Langer, J. Viefhaus, O. Hemmers, A. Menzel, R. Wehlitz, and U. Becker, Phys. Rev. A **43**, 1652 (1991).
[35] D. Nordfors (private communication).
[36] G. Angonoa and J. Schirmer (private communication).
[37] J. Feldhaus, W. Erlebach, A. L. D. Kilcoyne, K. J. Randall, and M. Schmidbauer, Rev. Sci. Instrum. **63**, 1454 (1992).
[38] E. Dietz, W. Braun, A. M. Bradshaw, and R. L. Johnson, Nucl. Instrum. Methods Phys. Res. Sect. A **239**, 359 (1985).
[39] F. Wuilleumier, Adv. X-Ray Anal. **16**, 63 (1973).
[40] D. W. Lindle, L. J. Medhurst, T. A. Ferrett, P. A. Heimann, M. N. Piancastelli, S. H. Liu, D. A. Shirley, T. A. Carlson, P. C. Deshmukh, G. Nasreen, and S. T. Manson, Phys. Rev. A **38**, 2371 (1988); U. Becker (private communication).
[41] H.-M. Köppe, A. L. D. Kilcoyne, J. Feldhaus, and A. M. Bradshaw (unpublished).
[42] R. R. Lucchese and V. McKoy, Phys. Rev. A **26**, 1406 (1982).
[43] D. L. Lynch and V. McKoy (private communication).
[44] B. L. Henke, P. Lee, T. J. Tanaka, R. L. Shimabukro, and B. K. Fujikawa, At. Data Nucl. Data Tables **27**, 1 (1982); B. L. Henke, E. M. Gullikson, and J. C. Davis, At. Data Nucl. Data Tables **54**, 181 (1993).
[45] R. McLaren, S. A. C. Clark, I. Ishii, and A. P. Hitchcock, Phys. Rev. A **36**, 1683 (1987).
[46] A. P. Hitchcock (private communication).
[47] At this photon energy the intensity of the secondary-electron background is small, hence a good fit to the satellite lines was possible (see Sec. V). Further, no shake-off electrons are produced, therefore only the satellite lines contribute to the total satellite intensity.
[48] C. M. Truesdale, D. W. Lindle, P. H. Kobrin, U. Becker, H. G. Kerkhoff, P. A. Heimann, T. A. Ferrett, and D. A. Shirley, J. Chem. Phys. **80**, 2319 (1984).
[49] J. Schirmer, M. Braunstein, and V. McKoy, Phys. Rev. A **41**, 283 (1990).
[50] R. R. Lucchese, G. Raseev, and V. McKoy, Phys. Rev. A **25**, 2572 (1982).
[51] R. R. Lucchese and V. McKoy, Phys. Rev. A **28**, 1382 (1983).
[52] J. L. Dehmer, D. Dill, and S. Wallace, Phys. Rev. Lett. **43**, 1005 (1979).
[53] T. K. Sham, B. X. Yang, J. Kirz, and J. S. Tse, Phys. Rev. A **40**, 652 (1989).
[54] M. N. Piancastelli, T. A. Ferrett, D. W. Lindle, L. J. Medhurst, P. A. Heimann, S. H. Liu, and D. A. Shirley, J.

Chem. Phys. **90**, 3004 (1989).
[55] M. N. Piancastelli, D. W. Lindle, T. A. Ferrett, and D. A. Shirley, J. Chem. Phys. **86**, 2765 (1987).
[56] H. M. Köppe, Doctoral thesis, Technische Universität Berlin, 1995 (unpublished).
[57] M. Schmidbauer, Doctoral thesis, Technische Universität Berlin, 1992 (unpublished).
[58] W. L. Jorgensen and L. Salem, *The Organic Chemist's Book of Orbitals* (Academic, New York, 1973).
[59] W. Eberhardt, J.-E. Rubensson, K. J. Randall, J. Feldhaus, A. L. D. Kilcoyne, A. M. Bradshaw, Z. Xu, P. D. Johnson, and Y. Ma, Phys. Scr. **T41**, 143 (1992).
[60] F. Larkins, Nucl. Instrum. Methods Phys. Res. Sect. B **87**, 215 (1994).
[61] H.-J. Freund, H. Kossmann, and V. Schmidt, Chem. Phys. Lett. **123**, 463 (1986).
[62] T. Porwol, G. Illing, H.-J. Freund, H. Kuhlenbeck, M. Neumann, S. Bernstorff, W. Braun, W. von Niessen, and C.-M. Liegener, Phys. Rev. B **41**, 10 510 (1990).
[63] W. Domcke, L. S. Cederbaum, J. Schirmer, W. von Niessen, C. E. Brion, and K. H. Tan, Chem. Phys. **40**, 171 (1979).
[64] J. A. Kelber, D. R. Jennison, and R. R. Rye, J. Chem. Phys. **75**, 652 (1981).
[65] G. E. Laramore, Phys. Rev. A **29**, 23 (1984).
[66] G. Bandarage and R. R. Lucchese, Phys. Rev. A **47**, 1989 (1993).